In-situ measurements and simulation of residual stresses and deformations in additively manufactured thin plates

Pouria Khanbolouki[a], Rodrigo Magana-Carranza[b], Chris Sutcliffe[c], Eann Patterson[b], John Lambros[a,1]

[a] *Department of Aerospace Engineering, University of Illinois, Urbana-Champaign, USA*

[b] *Department of Mechanical & Aerospace Engineering, University of Liverpool, UK*

[c] *Meta Consulting LDA, Portugal*

Abstract

In this work, the residual stresses and deformations developed during and after laser powder bed fusion (L-PBF) manufacture of thin quasi-2D metallic plates were investigated. Such thin structures are particularly susceptible to effects of residual stress development. A finite element analysis of the L-PBF process was validated with in-situ force measurements for the first time for a thin horizontal plate. The predicted forces developed reached a steady growth rate in the corners of the sample of 4.25 N per layer deposited, compared to 3.1 to 3.6 N per layer measured by in-situ load cells. The evolution of deformation and residual stress in a different configuration, thin vertical plates, during and after removal of support structures were also studied numerically and experimentally. Here, the finite element results showed good qualitative and quantitative (to within about 30% on average) agreement for residual deformations and final geometries of the thin vertical structures when compared with stereoscopic digital image correlation measurements. The results from the simulations showed that through-thickness stresses and shear stresses are

[1] Corresponding Author: Lambros@illinois.edu

negligible, while in-plane stresses grow in magnitude during the build process and the subsequent cooling period but are relaxed when the supporting structures are severed and the built plates removed from the base-plate, leaving tension in first built layers and compression in the last built layers. The models provide a tool for designing support structures and processes for release of the structures from their supports and substrates.

Keywords: Finite element analysis; In-situ force measurement; Digital image correlation; L-PBF; Thin plates

1. Introduction

Parts manufactured using laser powder bed fusion (L-PBF) are susceptible to build defects, and potentially failure, during the build process or in service, due to the residual stresses generated in manufacturing [1,2] which is a particular challenge for thin-walled parts. In L-PBF, a new layer of metal powder is deposited on the build substrate and consolidated through the use of a high-power laser which locally melts the powder. Melting of the newly deposited layer during the additive manufacturing (AM) process is accompanied by melting, local phase changes, and mechanical property gradients through the previously built layers, all of which are both temperature and time dependent. Upon solidification, the difference in the cool-down rates between the newly-melted and previously added layers results in residual tensile stresses [3]. For bulk objects manufactured using the L-PBF process, these residual stresses can be "locked-in" the microstructure and can lead to deformations of the build part at the macroscale upon release from the base plate, or substrate. If the object is large enough, and/or if it possesses axisymmetry, the presence of internal residual stresses is usually not detrimental to performance. In the case of thin quasi-two-dimensional structures built using L-PBF additive manufacturing, such residual stresses, primarily present in-plane, lead to out-of-plane deformations, and the absence of sufficient out-of-plane constraint from the underlying build increases the possibility of buckling [4]. Ultimately, out-of-plane deformation can cause excessive distortion, warping, or even failure in these quasi-two-dimensional structures. This reduces the potential applications of L-PBF as thin components, such as geometrically-reinforced rectangular panels used in several applications, including fusion reactors and hypersonic flight vehicles [5-7]. The manufacture of these structures with common machining and milling techniques from thicker stock plates can result in significant material waste [8], making additive manufacture of such structures an attractive alternative,

particularly when considering the substantial advantages of additive manufacturing, such as the ability to combine assembled components into a single part or the addition of unique features such as lattice geometries, smart surface structures or cooling channels/matrices.

Many techniques for measuring residual stresses are local [8] and, or destructive, e.g., hole drilling or layer removal [9,10]. Non-destructive alternatives, such as X-ray diffraction, exist although they generally only provide localized microstructural-level measurements [11]. Attempts have been made at full-field measurements of residual stress in AM parts with the use of neutron diffraction [12] or synchrotron X-ray diffraction [13], though these generally require specialized equipment [12]. In addition to the cost and accessibility of X-ray diffraction measurements, the results are limited to only measuring surface and near-surface residual stresses. In the present effort, we are interested in both the forces and deformation occurring over a large region of a structure, specifically a geometrically-reinforced L-PBF metal panel. An alternative for the study of the effects of residual stress, rather than measuring residual stresses themselves, is to monitor their "conversion" to a residual shape change after the build through full-field deformation measurements, for instance using Digital Image Correlation (DIC) or a coordinate measurement machine [13]. An understanding of the development of residual stresses requires knowledge of stresses induced during the build process which motivated our prior measurement work [4] and [15], and led us here to focus on predicting and understanding both the force measurements made *during* the build process and the full-field DIC deformation measurements *after* the build process for thin structures. Thin structures that lack rotational symmetry and, or have cross-sections in the build plane with large aspect ratios are particularly susceptible to distortion during and following the build process [4] and hence we have focused on enhancing our understanding of the mechanisms involved in generating residual stresses and the resultant distortion for such structures.

2. Background

Hashemi et al. [16] in their recent review of computational modelling of process-structure-property-performance relationships in metal additive manufacturing have classified models at micro-, meso- or macro-scale with the latter being of prime interest in understanding the gross deformation of large-scale structures induced by residual stress. In a more recent review, Sharma et al. [17] focused on multi-physics, multi-scale modelling of the thermofluid interactions in fusion-based additive manufacturing. A multi-physics simulation, incorporating the effects of local melt pool conditions and scan strategy can be valuable to gain a physical understanding of the additive manufacturing process at the microscale. However, such multi-physics solutions are numerically expensive for simulating entire components, and challenging to validate at the product scale, which is of interest here.

At the macro-scale, a wide range of quasi-standardized test geometries, such as cross-walls, wedges and canonical squares [26], L-shaped and bridge structures [19 & 27], and thick beams [28] have been used to explore the use of finite element models to predict residual stresses. Mohammedtaheri et al. [29] have reviewed the use of the modified inherent strain method, which is incorporated into many commercially-available finite element packages, to predict residual stresses in thin-walled structures and noted that the use of an enhanced layer lumping method avoided the underestimation of residual stresses. Similar conclusions were reached by Malmelöv et al. [30] using measurements of residual stress from synchrotron X-ray diffraction to validate their numerical modelling of a relatively thin vertical plate after calibrating their model using measurements of distortion in a multi-support beam. Zhou et al. [13] validated their finite element model of an Inconel 625 bridge structure built using laser powder bed fusion with measurements from neutron diffraction, X-ray diffraction, the contour method and a coordinate measurement

machine. They explored the effects pre-heating and of substrate removal which Mishutova et al. [31] found led to a redistribution of residual stresses and relaxation of parts built in Inconel 718, similarly to our earlier work [4]. Wheeler et al. [12] have deployed several finite element packages, including ABAQUS, ALE3D, ANSYS and COMSOL to model a thin-walled coupon and a hollow cylinder built using laser powder bed fusion in Inconel 625 and compared the predicted residual stresses with those measured using neutron diffraction. They found reasonable agreement between all of the packages and with the measurements, though Abarca et al. [32] found differences of ± 30% between predictions using ABAQUS and measurements from an optical scanner of a thin-walled half-cylinder with its axis in the build direction. The part was built using laser powder bed fusion in Ti-6Al-4V and the multi-scale model used a weakly coupled thermo-mechanical representation. While Jagatheeshkumar et al. [33] modelled the building, in Ti-6Al-4V, of thin cantilevers with their plane perpendicular to the build direction in laser powder bed fusion using ANSYS Additive Print and found that their predictions matched well with measurements from X-ray diffraction noting that low energy densities reduced residual stress and part distortion. In this work, we use the Additive suite by ANSYS [34] which uses a three-dimensional transient heat transfer description combined with a weakly coupled thermo-mechanical model to calculate the temperature fields, residual stresses, and deformations of geometrically-reinforced thin plates associated with the build process in laser powder bed fusion and with the removal of supports and removal of the part from the base-plate or substrate. Structures of this type are found in compressors, hypersonic flight vehicles and fusion energy reactors where they experience high temperature and broadband excitation.

It is helpful, and arguably necessary, to combine simulations with experimental measurements of both stresses and strains over the entire structure to clarify and predict the build

process for thin structures. Simulations are helpful in filling knowledge gaps in areas where direct in-situ or post-fabrication measurements are challenging, destructive, and/or expensive, such as for in-situ full-field deformation tracking during the build process, local residual stress measurements (such as the contour method, hole drilling, stripping method, nanoindentation) or full-field residual stress measurements at part-scale (such as diffraction methods) [35]. Here, the force evolution during the build and the deformation after the build are studied numerically and the results compared with the corresponding measurements based on our earlier experimental approaches reported in [4, 15, 36 & 37]. In [15] a unique experiment was conducted in which a custom-built force transducer device (FTD) mounted below an AM build was used to monitor the reaction forces during manufacture and cooling of a thin plate orientated so that the build direction was through its thickness. In [4], detailed full-field DIC measurements of the shape of a thin plate with its plane parallel to the build direction were made at the end of the build process, as well as during and after support removal. A focus of the present study is understanding the effects of the complex thermal processing history on the AM parts as the internal residual stresses created during the build process become shape changes (i.e., residual strains) during cool down and separation from the build platform. Thus, corresponding to the experiments of [4,15, 36 & 37], two sets of experimental builds and simulations have been performed: first, the in-situ forces during the additive manufacturing process were simulated and compared with the experimental measurements; and subsequently, the deformations of thin metallic plates after the L-PBF process, and during and after the part removal were calculated by FEA and compared with the full-field DIC measurements.

3. Experimental configurations and measurements

3.1 Force measurements during additive manufacture of a horizontal plate

In [13] Magana-Carranza et al. introduced an in-situ Force Transducer Device (FTD) to measure the forces exerted by a part during the build process [15 & 37]. A thin 64 × 64 × 3 mm Inconel-625 plate was built with its plane perpendicular to the build direction using L-PBF (Figure 1), i.e., the Z-direction. Sixteen load cells connected by individual rods to sixteen supports for the AM plate in a four-by-four array (Figure 1) formed the FTD. The FTD measured the spatial and temporal distribution of forces induced by the layer-by-layer addition of the material. The supports beneath the plate were inverted pyramids with square bases forming a plane on which the plate was built, and each support had a circular apex that attached to the top of a rod. The bottom of each rod was attached to a load cell in the form of a bending beam. First, the pyramidal supports were built on top of the connecting rods, and then the thin plate was built on top of the supports. Forces were first recorded as soon as the support structures were first connected to each other, i.e., corresponding to the first build layer of the thin plate being deposited. Forces were recorded with a sampling rate of 1,000 Hz for the rest of the build process until the maximum load capacity of the load cells was reached at which time the build process was stopped (~3 mm build height). Additional details of the load cell design and capabilities can be found in [15, 36 & 37].

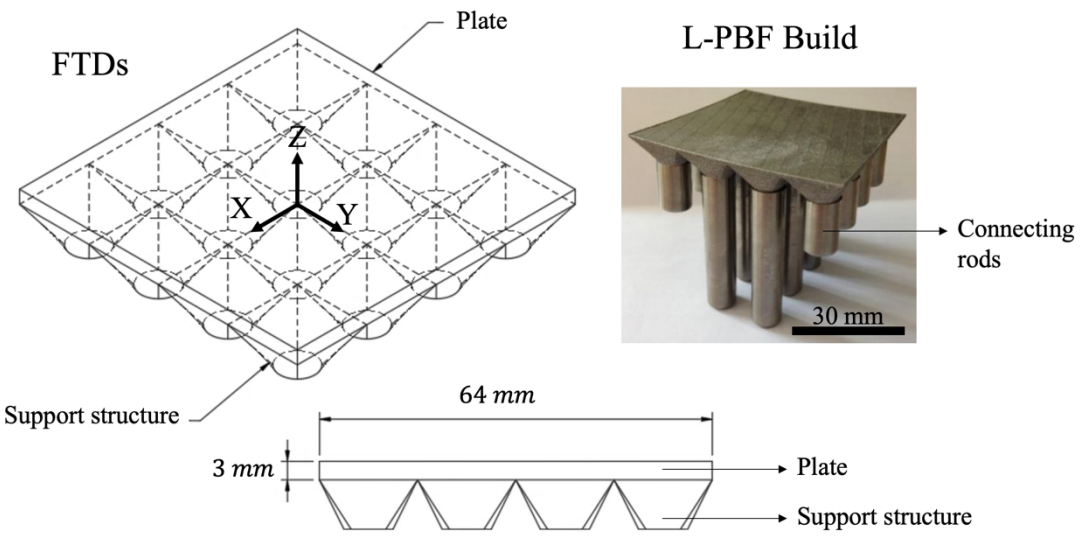

Figure 1 – Left and bottom: CAD model of the horizontal plate, including the 4×4 arrangement of inverted-pyramidal supports. Right: photograph of the L-PBF horizontal plate, inverted pyramidal supports and connecting rods after removal from the AM machine and load cells.

3.2 Residual deformation measurements after additive manufacture of a vertical plate

In [4], thin Inconel-625 plates 230 × 130 × 1.2 mm with a surrounding frame of 10 × 4.8 mm were built vertically in landscape and portrait orientations (Figure 2). To avoid plate failure during the build process, in-plane (X-Z plane) and out-of-plane (Y-Z plane) buttresses were added as reinforcements for builds in the portrait orientation, while only out-of-plane buttresses were needed for builds in the landscape orientation, see Figure 2. The build geometry also consisted of mounting holes in the frame for use in future thermo-acoustic experiments; however, these holes were omitted from the simulated geometry for simplification. The buttresses were connected to the frame of the plate with intermittently-spaced support structures as shown in Figure 2. On completion of the build, the resulting plate shape was measured at room temperature while still attached to the build platform using 3D-DIC. Subsequently, the plates were released from the

platform in incremental steps, starting with the buttresses and ending with the bottom connectors. The plate shape and deformation at every increment of support removal were recorded again using 3D-DIC. More details on the build procedure and the optical measurements can be found in [4]. An additional vertical plate in landscape mode was also prepared for this study to be compared with simulation results, see Figure 3. The landscape plate uses additional out-of-plane supports on the upper part of the frame for added stability during the manufacturing process.

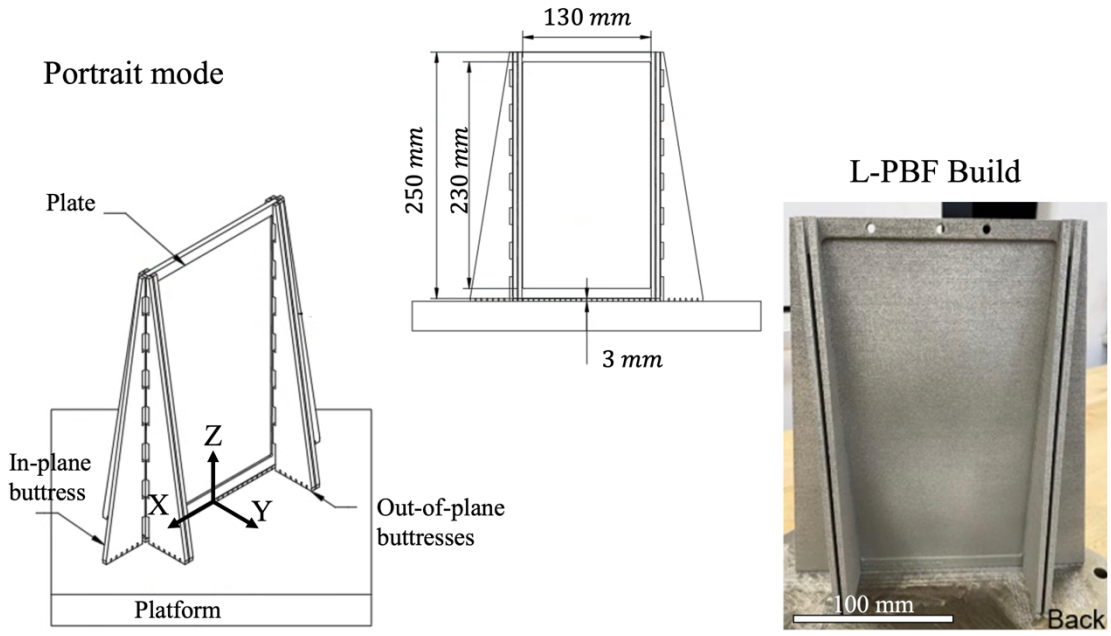

Figure 2 - Left: geometry of the vertical plate built in portrait orientation with buttresses. Right: photograph of the corresponding plate on the build platform.

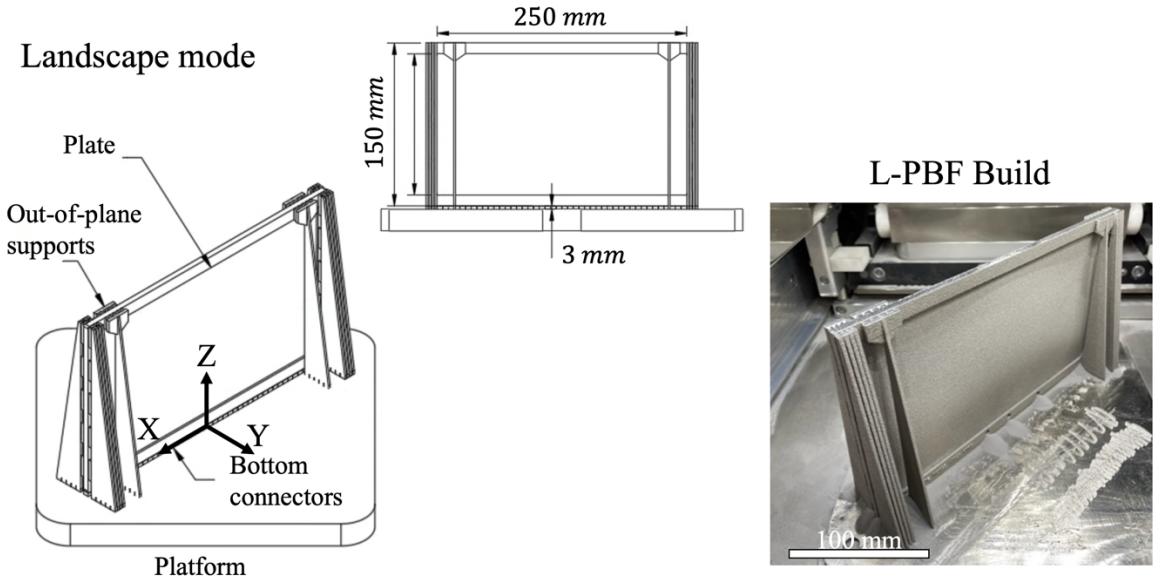

Figure 3 - Left: Geometry of the vertical plate in the landscape orientation with buttresses. Right: photograph of the corresponding plate on the build platform.

4. Thermal-structural simulations

Simulation of forces and residual deformations was performed using the ANSYS 2021R2 Additive Suite [34] with weakly coupled thermomechanical behaviour. In this scheme, a transient thermal history analysis was performed on the undeformed mesh in a layer-by-layer fashion with the results being used as the input for a static mechanical analysis. To optimize computational resources, the program lumped one or more physically-manufactured layers into one finite element layer, called a "super layer", by assuming that the thermal histories of the lumped layers were equivalent. To further simplify the simulation, this numerical scheme assumed that the X and Y direction thermal gradients were negligible with respect to the thermal gradients occurring in the build direction (Z-axis); hence, the laser scan strategies were not accounted for. Additionally, the effect of creep was neglected, as is common in similar simulations. To define the cooldown period between newly-deposited powder layers, a dwell time parameter was introduced. Dwell times of

8 and 10 seconds (Table 1) were chosen based on the laser on/off periods in the manufacturing process, though this difference in dwell time does not significantly alter the resulting build [38]. Element birth and death techniques were used to sequentially activate each super layer. The thermal interaction between the component and the surrounding powder medium was also modelled in a simplified fashion by using a convective heat transfer boundary condition. Other input parameters needed to perform the simulations included temperature-dependent material properties, for which the predefined material libraries provided by ANSYS for Inconel 625 were used, and the process-specific parameters listed in Table 1 from [4,15].

The support removal process can be approached in multiple ways. Some researchers have incorporated a one-step deactivation of the first layer of the mesh or the entire base plate after the build simulation has been executed [37]. Afazov et al. [21] implemented spring elements as support structures and simulated part removal from the base plate by deactivating the springs from the stiffness matrix. Here, an 'element birth and death' technique was employed to deactivate the support structures from the stiffness matrix. With this approach, we can conform to the customized geometries of the buttresses and support structure, including their effects on deformations and stresses of the plate during the build stage, in addition to specifying the sequence in which the supports were removed in the experimental studies. Finally, simulation times were reduced by making use of symmetry planes as shown in Figures 4-6.

Table 1 – Build parameters for the geometrically-reinforced plates taken from [4] and [15].

Simulation	In-situ Force Measurements (Horizontal Plates)	Deformation Measurements (Vertical Plates)
Deposition Thickness	6×10^{-2} mm	
Hatch Spacing	0.14 mm	
Scan Speed	600 mm/s	1750 mm/s
Dwell Time	10 s	8 s
Dwell Time Multiple	4	2
Number of Heat Sources	1	
Build conditions		
Preheat Temperature	22°C	170°C
Gas/Powder Temperature	Preheat Temperature	
Gas Convection Coefficient	10^{-5} W/mm²·°C	
Powder Convection Coefficient	10^{-5} W/mm²·°C	
Powder Property Factor	10^{-2}	
Cooldown Conditions		
Room Temperature	22°C	
Gas/Powder Temperature	Room Temperature	
Gas Convection Coefficient	10^{-5} W/mm²·°C	
Powder Convection Coefficient	10^{-5}W/mm²·°C	

3.1 Simulation of horizontal plate build

The simulations reproduced the geometry and processing conditions in [15] of the builds in which measurements were made with the in-situ FTD (Figure 4). Since no data were available for the forces exerted before the first layer of the plate was deposited, a decision was made to include the pyramidal supports as pre-built structures with no distortions so that, in effect, only the build process for the 3 mm plate was simulated. Since this is a through-thickness direction build of a thin plate, the height of the super layers was chosen to be equal to that of the physically deposited layers, i.e., in this case, the super layer consisted of one physically deposited layer in the AM build. The built part was meshed with layered tetrahedron (L-TET) elements with layer heights and lateral dimensions of 60 μm and 1.5 mm respectively. The same material properties

were used for both the horizontal plate and its support structure as provided by ANSYS material database for Inconel 625 [34]. The stiffness of the load cells and the rods connecting them to the pyramidal support structures was represented by elastic support boundary conditions in the build direction. These boundary conditions were based on the stiffness of the foundation in the physical system which was determined experimentally in [37]. Although in [37] a somewhat different stiffness was measured for each one of the 16 load cells, here we used an average spring coefficient of 1885 kPa based on the average from the measurements of [37] which has a range of ±214 kPa. More details on the experimental determination of the stiffness of the foundation are provided in [37]. Considering this spring coefficient value and the circular surface area of the connecting rods with a diameter of 8 mm, an average foundation stiffness of 37.5 N/mm^2 was applied to the bottom regions of the support structure. To fix the model in space, displacement boundary conditions were applied to the bottom surfaces of the support structure with the values in X and Y directions set to 0 mm. Finally, the inert gas and powder temperatures and convection coefficients were assumed to be 22 °C and 10^{-5} W/mm^{2}C respectively, and the default value (0.01) of the powder property factor[2] in ANSYS was used.

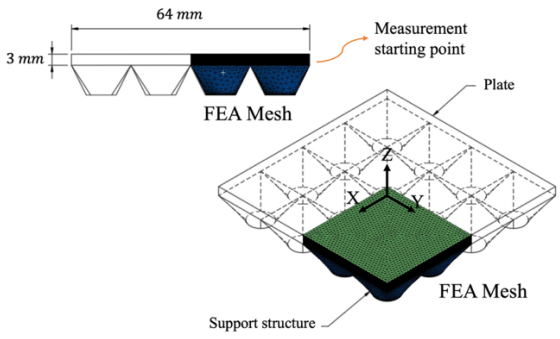

Figure 4 - The finite element model of the horizontal plate with supports showing the quarter-symmetry model meshed with layered tetrahedron elements.

[2] Powder-specific properties as a ratio to bulk solid properties used to account for heat transfer in the powder.

4.2 Simulation of vertical plate builds

The deformed shape of the geometrically-reinforced thin plates after the build and before and after support removal was simulated for plates built in both the portrait and landscape orientations, see Figures 5 and 6, using the properties listed in Table 1. Additionally, the steel base platform was included using predefined material properties provided by ANSYS for this material. In these simulations, the super layer height was 25× the physical layer height of 60 microns (i.e., each super layer was 1.5 mm) in order to save computational cost and time, since in this part of the study a much larger structure would be built. Note that in the support region super layers of 15× the physical layer height were used. In all cases the super layer values chosen were within the range recommended by ANSYS. While larger super layer heights can increase errors in calculating displacements, since the super layer height values were always within the recommended range, these errors are expected to be minimized. The plates and buttresses were represented by quadratic-layered tetrahedron elements with layer heights and lateral dimensions all equal to 1.5 mm. The connections between the geometrically-reinforced plate and the baseplate and buttresses were modelled with elements of dimensions 1 mm, while the base plate was modelled with elements of dimensions of 5 mm. Additionally, a variable layer height scheme was incorporated to decrease the overall simulation time by reducing the number of element-birth steps for the super layer. The first seven layers, where stress concentrations at the junctions of plate and bottom connectors could be high, were created individually with a super layer height of 1.5 mm per layer, followed by the simultaneous creation of three super layers at a time, i.e., 4.5 mm layer heights, for the rest of the build.

The buttresses were removed first from both sides, followed by incremental removal of the bottom connectors in 5 mm increments from either side towards the centre of the plate. The geometry used for this simulation uses half-symmetry boundary conditions. As a result, the removal of supports from either side occurred at the same time in the simulation, rather than sequentially as described in [4]. Frictionless boundary conditions in conjunction with perfectly insulated faces were applied to the nodes on the plane of symmetry. The boundary conditions for support structures in ANSYS are limited to the build direction (Z-axis). As a result, the out-of-plane and in-plane buttresses were defined with bonded contacts in X and Y directions as well as build-to-base bonds in Z direction [24]. Build-to-base bonds are a special type of bonded contact in the ANSYS Additive Suite, used for the bottom connectors, between the element faces of the bottom of the plate and the element faces of the top of the platform. The build parameters for the vertical plate simulations, both landscape and portrait orientations, similar to the experiments in [4] are shown in Table 1.

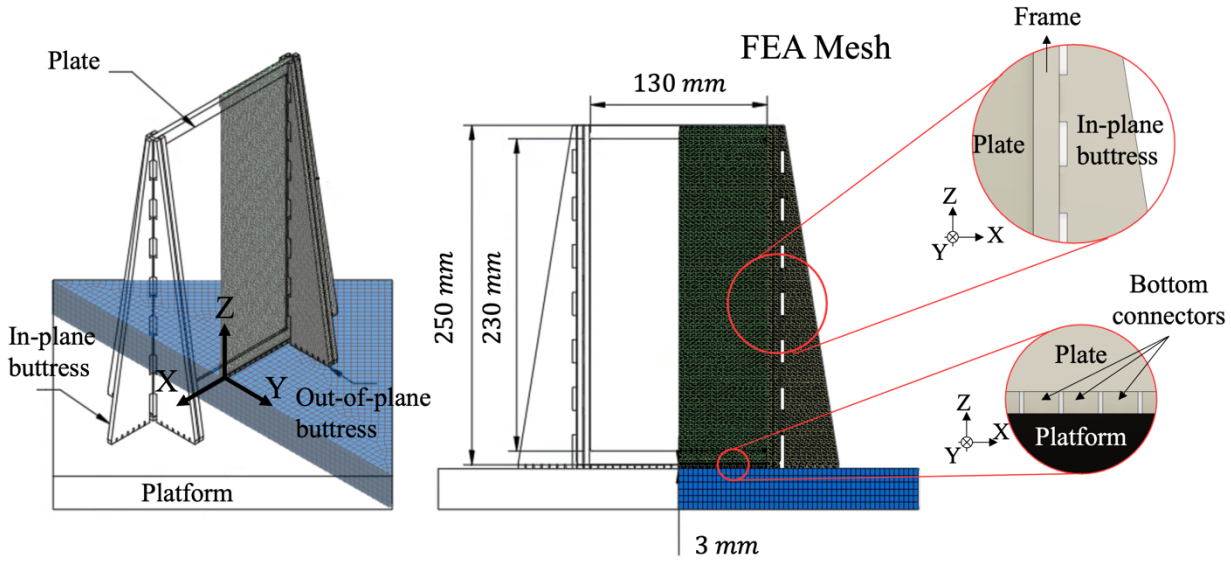

Figure 5 - The FEA model of the geometrically-reinforced plate built in the portrait orientation together with the buttresses meshed with layered tetrahedron elements throughout. Insets show the details of support structures at the bonding locations on the frame of the thin plate.

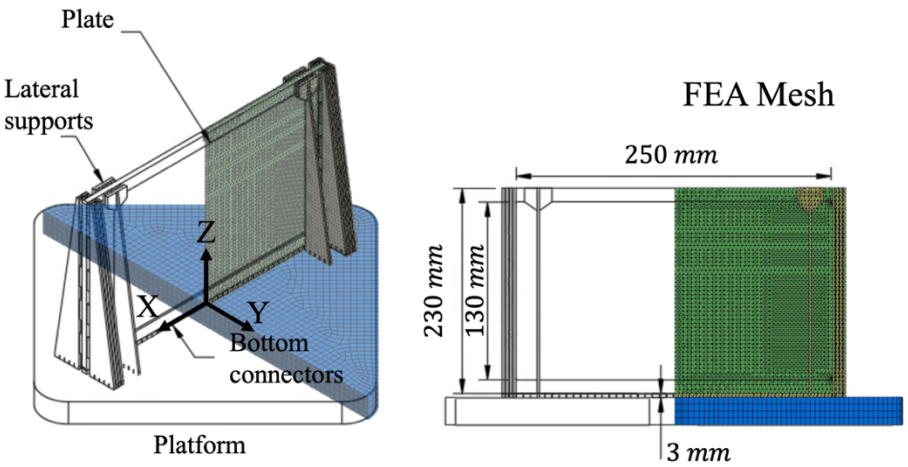

Figure 6 - The FEA model of the geometrically-reinforced plate built in landscape orientation together the buttresses meshed with layered tetrahedron elements.

5. Results and Discussion

5.1 In-situ force measurements

The measured and predicted results for the in-situ forces for the horizontal plate are shown in Figures 7 and 8. The FEA simulations were performed using a model with quarter symmetry; hence forces are predicted at four locations only, i.e., one corner, at the centre and on two edges. Note that the corner load cell forces are shown as negative and the centre forces as positive, although the plate curls upward at the corners since the simulation provides the forces on the pyramidal supports of the plate, i.e., the equal and opposite reaction to the force measured by the FTD in [15]. The experimental results, which correspond to 16 individual load cell locations, are plotted in the form of an average curve and a range as a function of both build time and layer

number in two graphs showing results for the edge locations separately from the remainder as there is a significant difference between the locations. In addition, in the simulations, there is no distinction between different scan strategies, of which two different ones, Meander and Stripe, were used in the experiments [4]. Therefore, Figures 7 and 8 show comparisons of the experimental results obtained using each of the two strategies with the same set of simulation results. A multi-physics simulation which can account for laser scan path would provide distinct simulation results for each scan strategy, and could furnish additional insight into the force evolution during L-PBF. However, such a framework is computationally much more expensive and can be challenging to validate at the macroscale of a built part, and thus was not used here.

It can be observed that the tensile forces at the corners are in equilibrium with the compressive forces in the centre regions of the plate. Predictions and measurements in Figures 7 and 8 show some agreement in terms of trends with both time during the build and spatially within the build as well as exhibiting approximately the same magnitude and sign. In addition, the FEA predictions capture the individual oscillations in force, seen in the measured forces which are related to the deposition of each successive layer; however, it is clear that the oscillations are smaller and have a decreasing magnitude over time, which is not seen in the measurements.

There are significant differences between the predictions and measurements for the edge of the plate where no significant forces are predicted numerically but forces as high as 200 N were measured in the first 15 layers of the build process. This difference might be a result of excluding any contributions of asymmetric effects, such as the influence of the laser scan strategy, in the simulation. The prediction also does not capture the rapid increase in force seen during the early stages of the build process when the first five to ten layers are being created. This difference between the measurements and simulations might have occurred because the simulation does not

capture the details of the initial stages in the deposition of material onto the pre-built support structure. At the start of the build for the thin plate, the pre-built support structure consists of a four-by-four array of individual supports with square top surfaces adjacent but not joined to each other. These supports are connected to one another by the deposition of the first and subsequent layers of the thin horizontal plate across the top of them and the stiffness of these connections will increase as more layers of the thin plate are added during the build. The load cells connected to the bottoms of the pre-built support structure will only sense residual forces in the thin plate when pre-built supports are connected together by the plate and initially these forces will be a function of the stiffness of these connections which will change rapidly as the first five to ten layers of the plate are built. This initial mechanism is not represented in the finite element model which probably accounts for the difference in results for initial ten layers, after which there is good agreement between force induced per layer during the build with values of 4.25 N per layer predicted by the simulation for the corners compared to about 3.6 and 3.1 N per layer measured by the corner load cells for the Stripe and Meander strategies respectively. In-situ measurement of distortions of a flexible substrate were performed by Dunbar et al. [39] at one location under the build platform with a microstrain measurement system. Their comparison with FEA simulations showed larger discrepancies of distortions between the experiment and simulations at the initial 1000 seconds of the build process as well. However, a detailed explanation of the initial discrepancies was not provided.

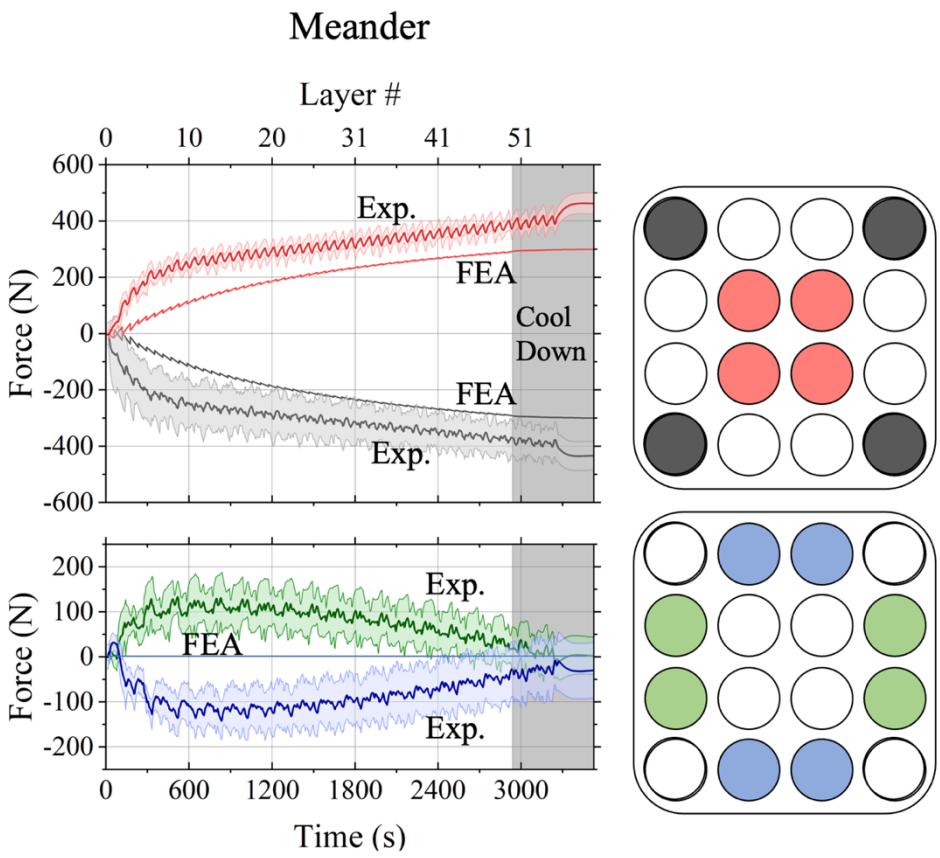

Figure 7 – Measured forces from [15] and predicted reaction forces during the build process and cooling period for the horizontal plate, 3 mm thick, built using the Meander scan strategy showing the spatial distribution of forces from the load cells in the corner (black lines), centre (red lines), and edges (blue and green lines) of the FTD. Experimental measurements are shown as an average curve and standard deviation from the four load cells belonging to each group (corner, centre, and edges).

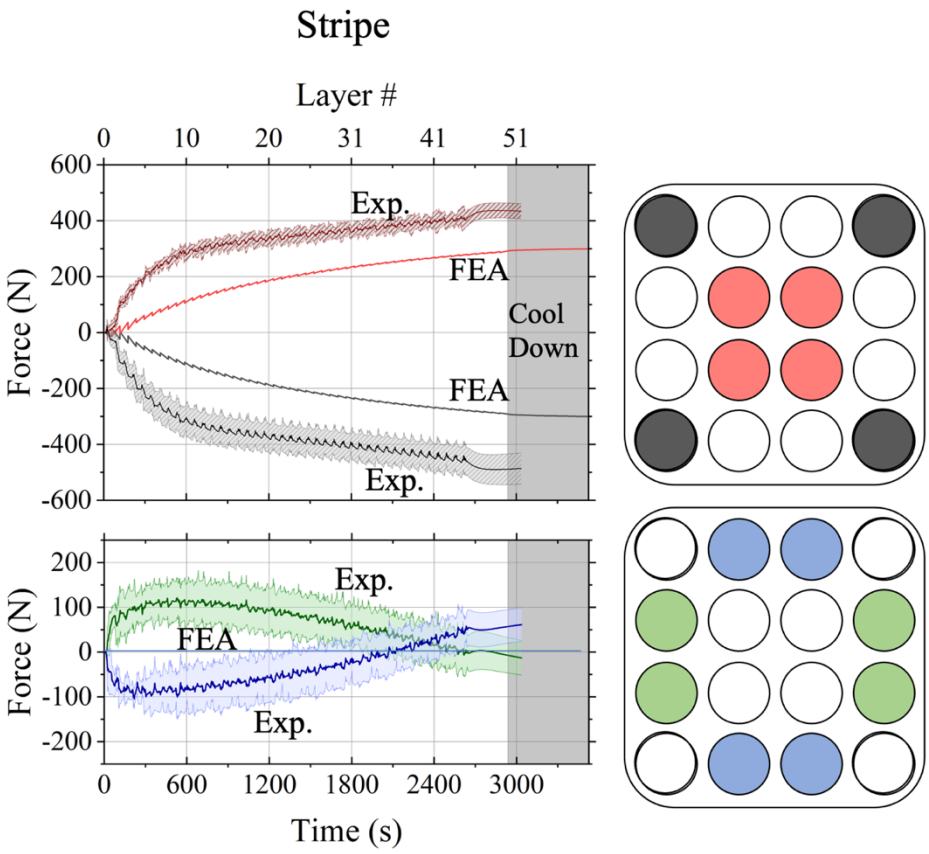

Figure 8 - Measured forces from [15] and predicted reaction forces during the build process and cooling period for the horizontal plate, 3 mm thick, built using the Stripe scan strategy showing the spatial distribution of forces from the load cells in the corner (black lines), centre (red lines), and edges (blue and green lines) of the FTD. Experimental measurements are shown as an average curve and standard deviation from the four load cells belonging to each group (corner, centre, and edges).

5.2 Deformations of geometrically-reinforced thin plates

Figure 9 shows a step-by-step view of the predicted out-of-plane displacements (ν) of the geometrically-reinforced vertical plate built in the portrait orientation during and after the manufacturing process, after cool-down, after the removal of buttresses, and after the complete

removal of the plate from the platform. It is evident that large out-of-plane deformations appear during the build stage and continue to accumulate and transform, i.e., there are changes in shape during the cut-off stages. While tracking the shape of the plate *in-situ* during the build step is very challenging experimentally and was not performed in [4], 3D-DIC was used to track the evolution of the shape of the plate after the build process, i.e., (a) immediately following cool down to room temperature, (b) following removal of the buttresses and (c) removal of the plate from the baseplate. The measured and predicted results for each of these three stages are shown in Figure 10 for the plate built in the portrait orientation and for the last stage only for the plate built in the landscape orientation in Figure 11. There is good overall agreement between the predictions and measurements which provides confidence in utilizing the finite element model to explore the evolution of residual stresses and resultant plate deformation as shown in Figure 9.

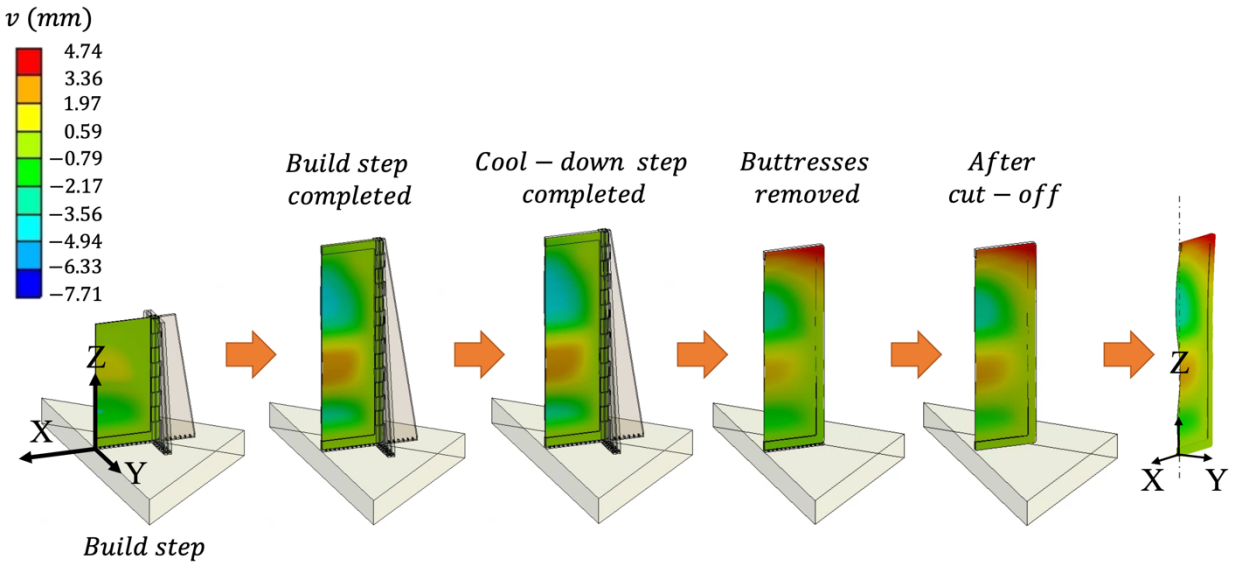

Figure 9 – Predicted out-of-plane deformation (v displacements) at stages of the manufacturing process for the geometrically-reinforced vertical plate built in the portrait orientation.

The measurements and predictions of the shape of the plate were very similar following both the cool-down and removal of the buttresses, although the predicted out-of-plane displacements were larger in both cases. When the plate was completely removed from the platform, the simulation predicted an extra half-wavelength of deformation along the centre vertical line resulting in an additional bulge adjacent to the bottom of the plate. These centerline profile shapes from experiments after cool-down, after buttress removal, and after complete plate removal from the platform are plotted together in Figure 12 and compared with their FEA counterparts. There is a good concordance between the predicted and measured deformed shapes; however, the prediction tends to overestimate the maximum deformations as mentioned earlier.

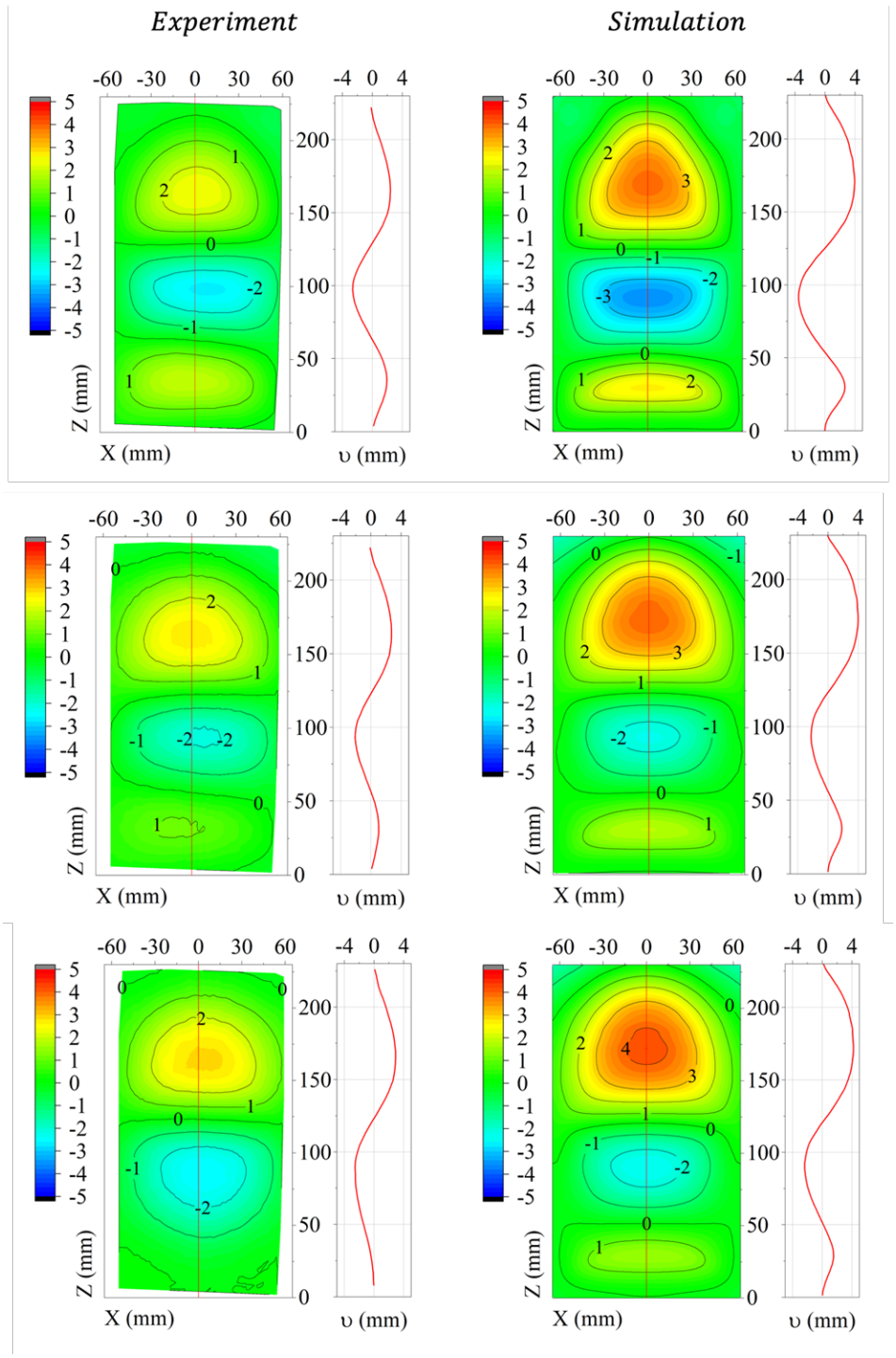

Figure 10 – Comparison of measurements [4] (left) and predictions (right) of out-of-plane deformation for the vertical plate, excluding the geometric reinforcement, at three stages in the manufacturing process: immediately following cooling to room temperature following building in

the portrait orientation (top); after removal of the buttresses (middle); and following removal from the baseplate (bottom). The line plots show the deformation along the vertical centerline (red line).

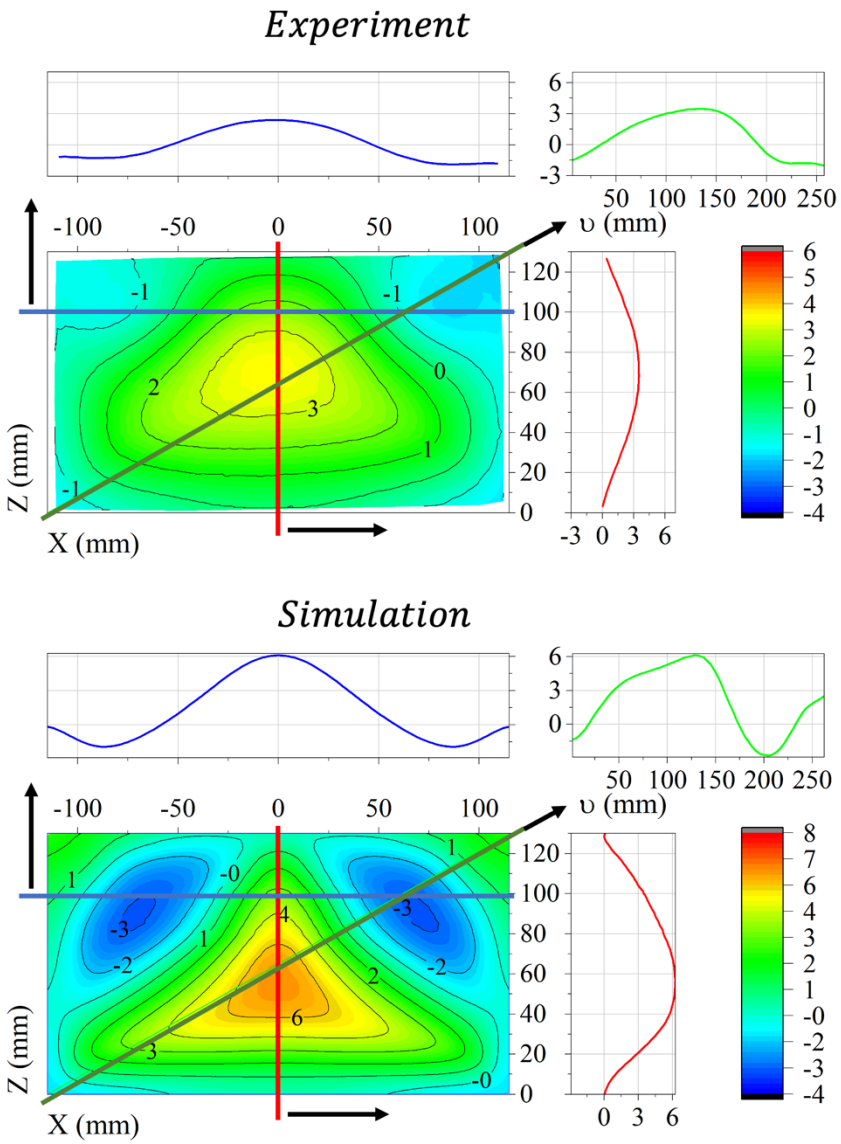

Figure 11 - Measurements (top) and predictions (bottom) of out-of-plane displacements for the vertical plate built in the landscape orientation after the part is fully removed from the build platform. Cross-sectional plots show the height maps along a diagonal (green), vertical (red), and horizontal (blue) directions of the contour maps.

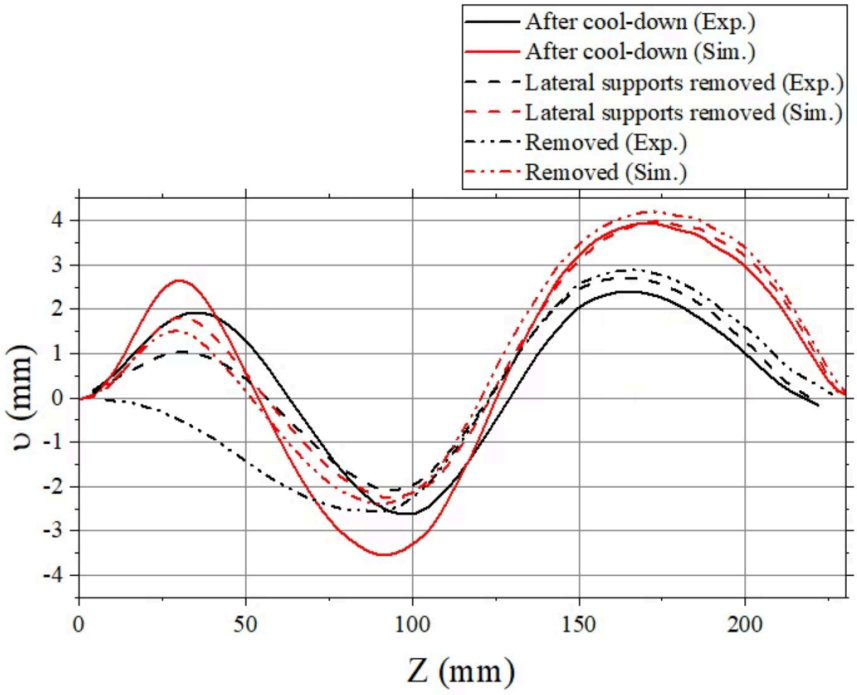

Figure 12 - Comparison of measurements and predictions of out-of-plane deformation along the centerline of the vertical plate built in the portrait orientation after cool-down, after the removal of lateral supports, and after the complete removal of the build.

5.3 Residual stress evolution

While the predicted deformations give us a direct and simple method for comparing experiments and simulations, understanding the mechanisms behind the distortions requires an analysis of the residual stresses. Although individual residual stress components cannot be easily measured, especially as they evolve through the build process, in section 5.1 it was shown that the model can capture the aggregate reaction forces with reasonable accuracy and, therefore, we can examine the predicted individual residual stresses from this numerical analysis with some degree of confidence. Figure 13 shows contour plots of normal stresses in the X-direction and Z-direction, σ_{xx} and σ_{zz} respectively, at the centre plane of the geometrically-reinforced vertical plate built in the portrait

orientation at various stages of the build process (from left to right): halfway through the build stage, at the end of the build stage, after cool-down, after buttress removal and after the complete cut-off. Note that all through thickness (i.e., Y-direction) stresses are negligible in comparison to the other stress components, and the *xz* shear stresses although present, are much less than σ_{xx} and σ_{zz} and are not shown. Figure 13 also shows line profiles of σ_{xx} and σ_{zz} at a height of 15 mm from the bottom of the plate. In the X-direction, the highest tensile stresses develop at the bottom region of the plate and gradually increase until the end of the cool-down step. The highest compressive stresses appear below the top frame of the plate towards the end of the process, with a slight increase during the cool-down step. Both the compressive and tensile stresses relax when the buttresses and bottom supports are removed. The highest compressive residual stresses in the build direction appear at the bottom center of the plate. The influence of this evolution of residual stress on plate deformation can be seen in the corresponding out-of-plane shapes shown in Figure 9.

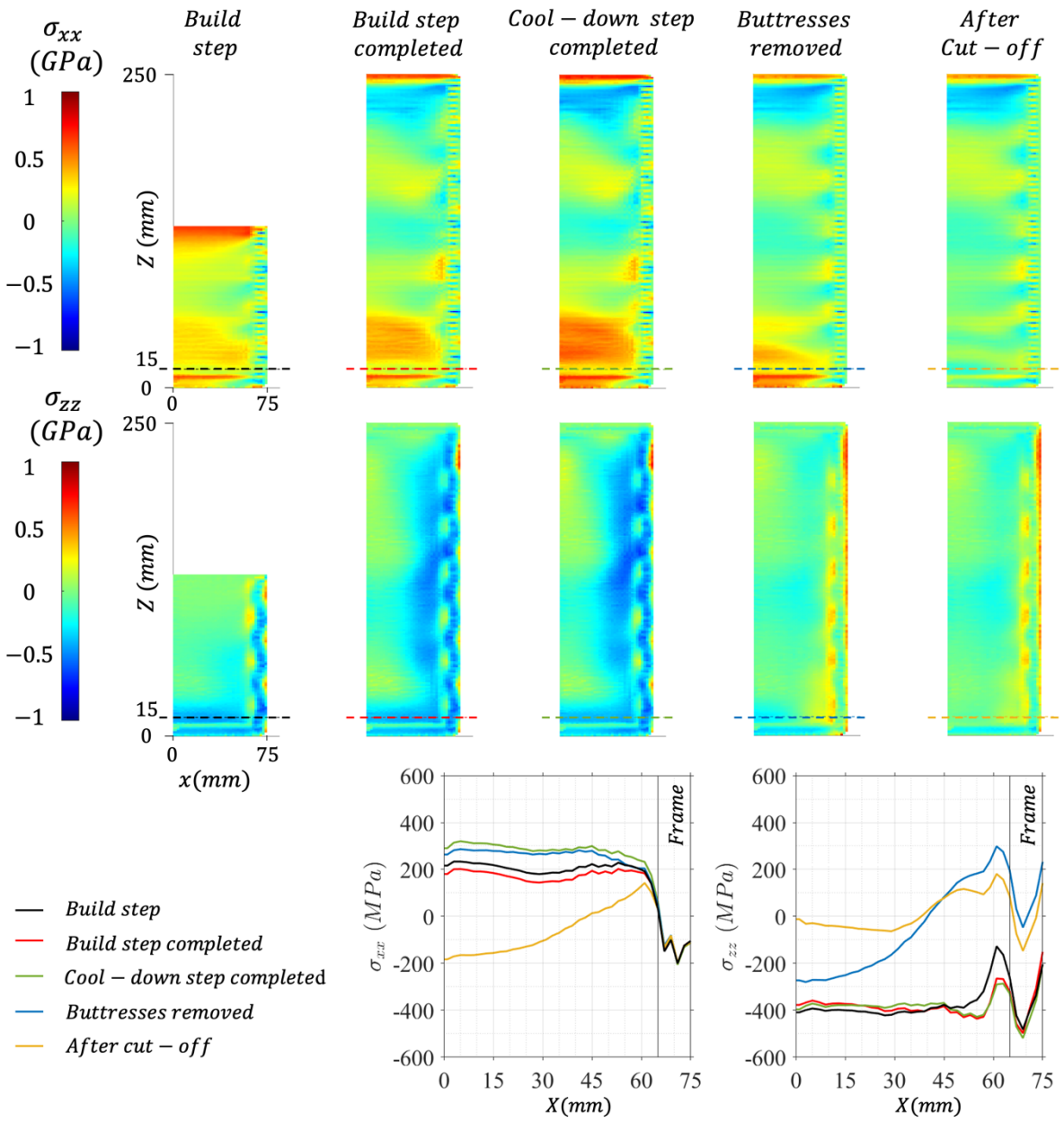

Figure 13 – Distribution of predicted normal residual stresses in the X-direction, σ_{xx} (top) and Z-direction, σ_{zz} (middle) for the vertical plate built in the portrait orientation at various stages of the build and cut-off process with corresponding line profiles at $z = 15$ mm (bottom).

Liu et al. studied the origins of residual stresses in terms of temperature gradient mechanisms using X-ray diffraction [40]. They concluded that compressive stresses occur at the bottom and tensile

stresses at the top of the geometries that were studied, i.e., closest and furthest from the build platform. Similar results are observed in Figure 13 until the last step of the support removal; when the removal of the supports led to a decrease in the residual stresses, σ_{zz} in the adjacent region of the plate. Similarly, the release of compressive residual stresses is observed at the prior step when the lateral in-plane and out-of-plane buttresses are removed. However, the affected regions are mostly along the side of the plate adjacent to the frame, where the lateral buttresses were previously attached. While Magana-Carranza [37] have also deduced that the high residual stress in the build direction gradually changes from tensile at the edges to compression at the center, these vertical quasi-2D plates show a more complex spatial residual stress development during the build and cut-off processes. This is indicative of the complex three-dimensional mechanisms at play during the build and removal of a quasi-2D structure and emphasizes the usefulness of implementing FEA to improve our understanding of the mechanisms inducing deformation and residual stresses during the additive manufacture of thin structures.

6. Conclusions

Using a combination of in-situ force measurements, ex-situ full-field deformation measurements, and finite elements analysis, this study has advanced our understanding of the large deformations and residual stresses developed during additive manufacturing using laser powder bed fusion (L-PDF) of quasi-2D thin metallic structures. A direct comparison between predictions from the finite element analysis and in-situ force measurements for a metallic structure has been performed for the first time. It was shown that the forces calculated from a weakly coupled thermo-mechanical lumped-layer approach generally were in good agreement with in-situ measurements. Simulations calculated a near-steady rate of force increase of 4.25 N per layer at the corners for

every layer printed after the first 10 layers deposited, as compared to measurements of 3.6 N per layer (for stripe laser scan) and 3.1 N per layer (for meander laser scan) from the experimental measurements. It was also shown that the simulations are capable of providing qualitative and quantitative (to within about 30% on average from Figure 12) predictions of residual deformations and final geometries of a thin plate structure. Additionally, simulations were able to capture the development of large out-of-plane deformations (between 2 mm–4 mm over the 250×150 mm vertical plates) during the build process of such structures without involving additional physics in the simulation scheme. The results from the simulations demonstrated that the through-thickness stresses and in-plane shear stresses in the thin plates were negligible compared to other stress components. The normal in-plane stresses perpendicular to the build direction adjacent to the base-plate were found to be tensile and to increase until the end of the cool-down stage while at the top of the plate they were compressive at the end of the build process. All of the in-plane normal stresses relaxed as the buttresses and connections to the base-plate were removed resulting in compressive stresses in the lower sections of the plate and substantial deviation of the plates from flatness.

Declarations

Credit author statement

Methodology, formal analysis, and visualization were performed by Pouria Khanbolouki. Experimental investigation and data curation were performed by Rodrigo Magana-Carranza. Conceptualization, supervision, and funding acquisition were performed by Chris Sutcliffe, Eann Patterson, and John Lambros. The first draft of the manuscript was written by Pouria Khanbolouki

and all authors commented on previous versions of the manuscript. Pouria Khanbolouki, Chris Sutcliffe, Eann Patterson, and John Lambros read, edited, and approved the final manuscript.

Funding

The research was supported by grants from both the EPSRC (grant no. EP/T013141/1) in the UK and NSF CMMI (grant no. 20–27082) in the USA.

Statement of competing interests

The authors have no relevant financial or non-financial interests to disclose.

References:

1. Gisario, M. Kazarian, F. Martina and M. Mehrpouya, "Metal additive manufacturing in the commercial aviation industry: A review," *Journal of Manufacturing Systems,* vol. 53, pp. 124-149, 2019.
2. M. Brennan, J. Keist and T. Palmer, "Defects in Metal Additive Manufacturing Processes," *Journal of Materials Engineering and Performance,* no. 30, p. 4808–4818, 2021.
3. S.-G. Chen, H.-j. Gao, Q. Wu, Z.-h. Gao and X. Zhou, "Review on residual stresses in metal additive manufacturing: formation mechanisms, parameter dependencies, prediction and control approaches," *Journal of Materials Research and Technology,* 2022.
4. E. A. Patterson, J. Lambros, R. Magana-Carranza and C. J. Sutcliffe, "Residual stress effects during additive manufacturing of reinforced thin nickel–chromium plates," *The International Journal of Advanced Manufacturing Technology,* pp. 1-13, 2022.
5. V. T. Le, N. S. Goo and J. Y. Kim, "Thermomechanical behavior of superalloy thermal protection system under aerodynamic heating," *Journal of Spacecraft and Rockets,* vol. 56, no. 5, pp. 1432-1448, 2019.
6. Y.-Z. Yang, J.-l. Yang and D.-n. Fang, "Research progress on thermal protection materials and structures of hypersonic vehicles," *Applied Mathematics and Mechanics,* vol. 29, pp. 51-60, 2008.
7. K. D. Ramkumar, S. Dev, V. Saxena, A. Choudhary, N. Arivazhagan and S. Narayanan, "Effect of flux addition on the microstructure and tensile strength of dissimilar weldments involving Inconel 718 and AISI 416," *Materials & Design,* vol. 87, pp. 663-674, 2015.
8. B. Blakey-Milner, P. Gradl, G. Snedden, M. Brooks, J. Pitot, E. Lopez, M. Leary, F. Berto and A. d. Plessis, "Metal additive manufacturing in aerospace: A review," *Materials & Design,* no. 209, p. 110008, 2021.
9. E. Denlinger, J. Heigel, P. Michaleris and T. Palmer, "Effect of inter-layer dwell time on distortion and residual stress in additive manufacturing of titanium and nickel alloys," *Journal of Materials Processing Technology,* vol. 215, pp. 123-131, 2015.

10. E.-9. A. Standard, *Standard Test Method for Determining Residual Stresses by the Hole-Drilling Strain-Gage Method,* Philadelphia, PA: American Society for Testing and Materials, 1992.
11. J. Schröder, A. Evans, T. Mishurova, A. Ulbricht, M. Sprengel, I. Serrano-Munoz, T. Fritsch, A. Kromm, T. Kannengießer and G. Bruno, "Diffraction-based residual stress characterization in laser additive manufacturing of metals," *Metals,* vol. 11, no. no. 11, p. 1830, 2021.
12. Wheeler, K., Gnaupel-Herold, T., Ellis, D., Hafiychuk, V., Aires, J., Gee, K. and Hafiychuk, H., Residual Stress Measurement and Comparison to Model Predictions for Alloy 625 Laser Powder Bed Fusion Additive Manufacturing Samples. *Available at SSRN 4062355.*
13. Zhou, J., Barrett, R.A. and Leen, S.B., 2023. Finite element modelling for mitigation of residual stress and distortion in macro-scale powder bed fusion components. *Proceedings of the Institution of Mechanical Engineers, Part L: Journal of Materials: Design and Applications*, *237*(6), pp.1458-1474.
14. T. Q. Phan, M. Strantza, M. R. Hill, T. H. Gnaupel-Herold, J. Heigel, C. R. D'Elia, A. T. DeWald, B. Clausen, D. C. Pagan, J. Y. P. Ko, D. W. Brown and L. E. Levine, "Elastic residual strain and stress measurements and corresponding part deflections of 3D additive manufacturing builds of IN625 AM-bench artefacts using neutron diffraction, synchrotron X-ray diffraction, and contour method," *Integrating Materials and Manufacturing Innovation,* no. 8, pp. 318-334, 2019.
15. R. Magana-Carranza, C. J. Sutcliffe and E. A. Patterson, "The effect of processing parameters and material properties on residual forces induced in Laser Powder Bed Fusion (L-PBF)," *Additive Manufacturing,* no. 46, p. 102192, 2021.
16. Hashemi, S.M., Parvizi, S., Baghbanijavid, H., Tan, A.T., Nematollahi, M., Ramazani, A., Fang, N.X. and Elahinia, M., 2022. Computational modelling of process–structure–property–performance relationships in metal additive manufacturing: A review. *International Materials Reviews*, *67*(1), pp.1-46.
17. Sharma, S., Joshi, S.S., Pantawane, M.V., Radhakrishnan, M., Mazumder, S. and Dahotre, N.B., 2023. Multiphysics multi-scale computational framework for linking process–structure–property relationships in metal additive manufacturing: a critical review. *International Materials Reviews*, pp.1-67.
18. P. M. E. D. J. I. Michael Gouge, "Chapter 2 - The Finite Element Method for the Thermo-Mechanical Modeling of Additive Manufacturing Processes," in *Thermo-Mechanical Modeling of Additive Manufacturing*, Butterworth-Heinemann, 2018, pp. 19-38.
19. C. Li, Z. Y. Liu, X. Y. Fang and Y. B. Guo, "On the simulation scalability of predicting residual stress and distortion in selective laser melting," *Journal of Manufacturing Science and Engineering,* vol. 140, no. no. 4, 2018.
20. C. Li, C. H. Fu, Y. B. Guo and F. Z. Fang, "A multiscale modelling approach for fast prediction of part distortion in selective laser melting," *Journal of Materials Processing Technology,* vol. 229, pp. 703-712, 2016.
21. S. Afazov, W. A. Denmark, B. L. Toralles, A. Holloway and A. Yaghi, "Distortion prediction and compensation in selective laser melting," *Additive Manufacturing,* vol. 17, pp. 15-22, 2017.
22. M. F. Zaeh and G. Banner, "Investigations on residual stresses and deformations in selective laser melting," *Prod. Eng. Res. Devel.,* vol. 4, p. 35–45, 2010.

23. E. R. Denlinger, M. Gouge, J. Irwin and P. Michaleris, "Thermomechanical model development and in situ experimental validation of the Laser Powder-Bed Fusion process," *Additive Manufacturing,* vol. 16, pp. 73-80, 2017.
24. C. Li, E. R. Denlinger, M. F. Gouge, J. E. Irwin and P. Michaleris, "Numerical verification of an Octree mesh coarsening strategy for simulating additive manufacturing processes.," *Additive Manufacturing,* vol. 30, p. 100903, 2019.
25. N. Keller and V. Ploshikhin, "New Method for Fast Predictions on Residual Stress and Distortion of AM Parts," in *International Solid Freeform Fabrication Symposium*, University of Texas at Austin, 2014.
26. T. Mayer, G. Brändle, A. Schönenberger and R. Eberlein, "Simulation and validation of residual deformations in additive manufacturing of metal parts," *Heliyon,* vol. 6, no. no. 5, p. e03987, 2020.
27. J.-P. Kruth, J. Deckers, E. Yasa and R. Wauthlé, "Assessing and comparing influencing factors of residual stresses in selective laser melting using a novel analysis method," *Proceedings of the Institution of Mechanical Engineers, Part B: Journal of Engineering Manufacture,* vol. 226, no. no. 6, pp. 980-991, 2012.
28. Kaess, M., Werz, M. and Weihe, S., 2023. Residual Stress Formation Mechanisms in Laser Powder Bed Fusion—A Numerical Evaluation. *Materials*, *16*(6), p.2321.
29. Mohammadtaheri, H., Sedaghati, R. and Molavi-Zarandi, M., 2022. Inherent strain approach to estimate residual stress and deformation in the laser powder bed fusion process for metal additive manufacturing—a state-of-the-art review. *The International Journal of Advanced Manufacturing Technology*, *122*(5-6), pp.2187-2202
30. Malmelöv, A., Hassila, C.J., Fisk, M., Wiklund, U. and Lundbäck, A., 2022. Numerical modeling and synchrotron diffraction measurements of residual stresses in laser powder bed fusion manufactured alloy 625. *Materials & design*, *216*, p.110548
31. T. Mishurova, S. Cabeza, K. Artzt, J. Haubrich, M. Klaus, C. Genzel, G. Requena, G. Bruno, An assessment of subsurface residual stress analysis in SLM Ti-6Al4V, Materials (Basel). 10 (4) (2017) 348
32. Abarca, M.J., Darabi, R., de Sa, J.C., Parente, M. and Reis, A., 2023. Multi-scale modelling modeling for prediction of residual stress and distortion in Ti-6Al-4V Ti–6Al–4V semi-circular thin-walled parts additively manufactured by laser powder bed fusion (LPBF). *Thin-Walled Structures*, *182*, p.110151.
33. S. Jagatheeshkumar, M. Raguraman, S. P. AVS, B. K. Nagesha and U. Chandrasekhar, " Study of residual stresses and distortions from the Ti6Al4V based thin-walled geometries built using LPBF process," *Defence Technology,* 2023.
34. "Ansys Additive Manufacturing Solutions," ANSYS, Inc, 2023. [Online]. Available: https://www.ansys.com/products/additive.
35. G. U. O. Jiang, F. U. Haiyang, P. A. N. Bo and K. A. N. G. Renke, "Recent progress of residual stress measurement methods: A review," *Chinese Journal of Aeronautics,* vol. 34, no. no. 2, pp. 54-78., 2021.
36. R. M. Carranza, J. Robinson, I. Ashton, P. Fox, C. Sutcliffe and E. Patterson, " A novel device for in-situ force measurements during laser powder bed fusion (L-PBF)," *Rapid Prototyping Journal,* vol. 27, no. no. 7, pp. 1423-1431, 2021.
37. R. M. Carranza, "Determination of residual stress in components manufactured using laser powder bed fusion (L-PBF).," The University of Liverpool, United Kingdom, 2020.

38. Shrivastava, Abhishek, S. Anand Kumar, and Samrat Rao. "A numerical modelling approach for prediction of distortion in LPBF processed Inconel 718." *Materials Today: Proceedings*44 (2021): 4233-4238.
39. Dunbar, A.J., Denlinger E.R., Gouge M.F., Michaleris P. "Experimental validation of finite element modeling for laser powder bed fusion deformation." *Additive Manufacturing* 12 (2016): 108-120.
40. Y. Liu, Y. Yang and D. Wang, " A study on the residual stress during selective laser melting (SLM) of metallic powder," *The International Journal of Advanced Manufacturing Technology,* vol. 87, pp. 647-656, 2016.